Article

Theory of 1,3-Dipolar Cycloadditions: Distortion/Interaction and Frontier Molecular Orbital Models

Daniel H. Ess, and K. N. Houk

J. Am. Chem. Soc., **2008**, 130 (31), 10187-10198 • DOI: 10.1021/ja800009z • Publication Date (Web): 10 July 2008

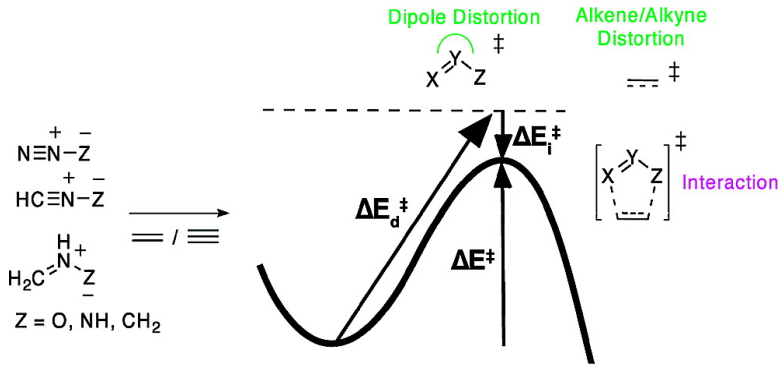

More About This Article

Additional resources and features associated with this article are available within the HTML version:

- Supporting Information
- Links to the 2 articles that cite this article, as of the time of this article download
- Access to high resolution figures
- Links to articles and content related to this article
- Copyright permission to reproduce figures and/or text from this article

View the Full Text HTML

J|A|C|S
ARTICLES

Published on Web 07/10/2008

Theory of 1,3-Dipolar Cycloadditions: Distortion/Interaction and Frontier Molecular Orbital Models

Daniel H. Ess and K. N. Houk*

Department of Chemistry and Biochemistry, University of California, Los Angeles, California 90095

Received January 2, 2008; E-mail: houk@chem.ucla.edu

Abstract: Quantum chemical calculations of activation barriers and reaction energies for 1,3-dipolar cycloadditions by the high-accuracy CBS-QB3 method reveal previously unrecognized quantitative trends in activation barriers. The distortion/interaction model of reactivity explains why (1) there is a monotonic decrease of ~6 kcal/mol in the activation energy along the series oxides, imine, and ylide for the diazonium, nitrilium, and azomethine betaine classes of 1,3-dipoles; (2) nitrilium and azomethine betaines with the same trio of atoms have almost identical cycloaddition barrier heights; (3) barrier heights for the cycloadditions of a given 1,3-dipole with ethylene and acetylene have the same activation energies (mean absolute deviation of 0.6 kcal/mol) in spite of very different reaction thermodynamics ($\Delta\Delta H_{rxn}$ range = 14−43 kcal/mol) and frontier molecular orbital (FMO) energy gaps. The energy to distort the 1,3-dipole and dipolarophile to the transition state geometry, rather than FMO interactions or reaction thermodynamics, controls reactivity for cycloadditions of 1,3-dipoles with alkenes or alkynes. A distortion/interaction energy analysis was also carried out on the transition states for the cycloadditions of diazonium dipoles with a set of substituted alkenes (CH_2CHX, X = OMe, Me, CO_2Me, Cl, CN) and reveals that FMO interaction energies between the 1,3-dipole and the dipolarophile differentiate reactivity when transition state distortion energies are nearly constant.

Introduction

1,3-Dipolar cycloadditions have a tremendously successful history of use in heterocycle synthesis[1] but are now utilized in almost every area of chemistry, including, materials chemistry,[2] drug discovery,[3] and chemical biology.[4] The 1,3-dipole is typically represented by closed-shell all-octet valence structures, $X{=}Y^+{-}Z^- \leftrightarrow X^-{-}Y^+{=}Z$. They range from the very familiar atmospheric components, ozone (O_3) and nitrous oxide (N_2O), to the highly popular azides (N_3R) of Click chemistry.[5] The $[{}_\pi4_s + {}_\pi2_s]$ thermal cycloadditions of 1,3-dipoles with alkene and alkyne dipolarophiles generate five-membered heterocycles and are called 1,3-dipolar cycloadditions because of the dipolar nature of the principal resonance structures and the 1,3-additions that they undergo (Scheme 1).[6,7]

Scheme 1. General 1,3-Dipolar Cycloaddition and Possible X, Y, and Z Combinations from First-Row Atoms

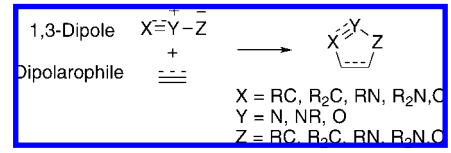

The most successful qualitative reactivity[8] and selectivity[9] model for 1,3-dipolar cycloadditions is based on frontier molecular orbital (FMO) theory,[10,11] commonly involving approximate quantum mechanical methods and electronic properties of isolated reactants.[12] This theory concentrates on

(1) *Synthetic Applications of 1,3-Dipolar Cycloaddition Chemistry Toward Heterocycles and Natural Products*; Padwa, A.; Pearson, W. H., Eds.; Wiley: New York, 2002.
(2) (a) Collman, J. P.; Devaraj, N. K.; Chidsey, C. E. D. *Langmuir* **2004**, *20*, 1051. (b) Speers, A. E.; Adam, G. C.; Cravatt, B. F. *J. Am. Chem. Soc.* **2003**, *125*, 4686.
(3) Krasinski, A.; Radic, Z.; Manetsch, R.; Raushel, J.; Taylor, P.; Sharpless, K. B.; Kolb, H. C. *J. Am. Chem. Soc.* **2005**, *127*, 6686.
(4) Seo, T. S.; Bai, X.; Ruparel, H.; Li, Z.; Turro, N. J.; Ju, J. *Proc. Natl. Acad. Sci. USA* **2004**, *101*, 5488.
(5) Kolb, H. C.; Finn, M. G.; Sharpless, K. B. *Angew. Chem., Int. Ed.* **2001**, *40*, 2004.
(6) (a) Huisgen, R. *Angew. Chem. Chem., Int. Ed. Engl.* **1963**, *2*, 565. (b) Huisgen, R. *Angew. Chem. Chem., Int. Ed. Engl.* **1963**, *2*, 633. (c) Huisgen, R. *Angew. Chem. Chem., Int. Ed. Engl.* **1968**, *7*, 321. (d) Huisgen, R. In *1,3-Dipolar Cycloaddition Chemistry*; Padwa, A., Ed.; John Wiley and Sons: New York, 1984; Vol. 1.
(7) Woodward, R. B.; Hoffmann, R. *Angew. Chem., Int. Ed. Engl.* **1969**, *8*, 781.
(8) (a) Sustmann, R. *Tetrahedron Lett.* **1971**, *12*, 2717. (b) Sustmann, R.; Trill, H. *Angew. Chem. Chem., Int. Ed. Engl.* **1972**, *11*, 838. (c) Houk, K. N. In *1,3-Dipolar Cycloaddition Chemistry*; Padwa, A., Ed.; John Wiley and Sons: New York, 1984; Vol. 2.
(9) (a) Houk, K. N.; Sims, J.; Duke, R. E., Jr.; Strozier, R. W.; George, J. K. *J. Am. Chem. Soc.* **1973**, *95*, 7287. (b) Houk, K. N.; Sims, J.; Watts, C. R.; Luskus, L. J. *J. Am. Chem. Soc.* **1973**, *95*, 7301. (c) Bastide, J.; Ghandour, W. E.; Henri-Rousseau, O. *Tetrahedron Lett.* **1972**, *41*, 4225.
(10) (a) Salem, L. *J. Am. Chem. Soc.* **1968**, *90*, 543. (b) Salem, L. *J. Am. Chem. Soc.* **1968**, *90*, 553.
(11) (a) Fukui, K. *Acc. Chem. Res.* **1971**, *4*, 57. (b) Houk, K. N. *Acc. Chem. Res.* **1975**, *8*, 361. (c) Houk, K. N. In *Pericyclic Reactions*; Marchand, A. P.; Lehr, R. E., Eds.; Academic Press: New York, 1977; Vol. 2, p 181. (d) Fukui, K. *Angew. Chem., Int. Ed. Engl.* **1982**, *21*, 801.
(12) For recent uses of FMO theory for 1,3-dipolar cycloadditions, see: (a) Jikyo, T.; Schatz, J.; Maas, G. *J. Phys. Org. Chem.* **2003**, *16*, 504. (b) Marakchi, K.; Kabbaj, O.; Komiha, N.; Jalal, N.; Esseffar, M. *J. Mol. Struct. (THEOCHEM)* **2003**, *620*, 271. (c) Domingo, L. R.; Benchouk, W.; Mekelleche, S. M. *Tetrahedron* **2007**, *63*, 4464. (d) Li, X-B.; Song, Q-H. *Heteroat. Chem* **2007**, *3*, 203.

Scheme 2. Concerted and Stepwise Mechanisms for 1,3-Dipolar Cycloadditions

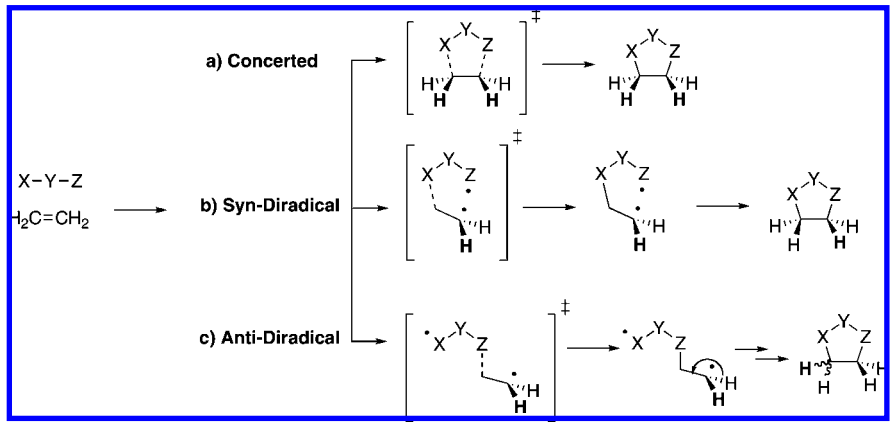

the relative reactivity and regioselectivity of a series of substituted alkenes toward a given 1,3-dipole. Conceptual density functional theory and configuration mixing have also been applied to understanding cycloaddition reactivity.[13] Cycloaddition reactivity has also been discussed in terms of thermodynamic effects[14] by using well-known reactivity−thermodynamic relationships from Evans-Polanyi,[15] Brønsted,[16] and Marcus.[17] Recently, based on new high-accuracy quantum mechanical calculations using the CBS-QB3 multicomponent method, we proposed a new distortion/interaction energy model for 1,3-dipolar cycloaddition reactivity.[18] Herein we give a full report of this model based on activation and reaction enthalpies computed for dipoles **1**−**9** (shown below) with ethylene and acetylene.

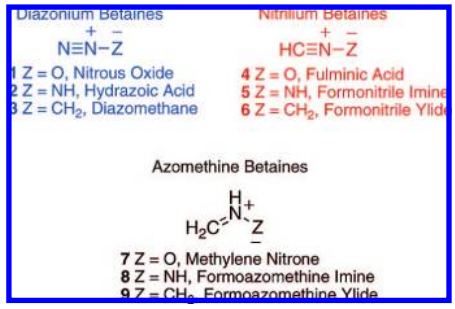

Background. In the late 1950s, Rolf Huisgen undertook a general study of diazoalkane additions to strained double bonds.[6] This study ultimately expanded to the generalization and classification of 1,3-dipolar cycloadditions. For so-called 1,3-dipoles "with a double bond," atoms X and Z can be C, N, or O, while the center atom Y is nitrogen. These are typically referred to as propargylic species and have two sets of degenerate π-orbitals in a linear structure. Dipoles "without a double bond" may have a nitrogen function or oxygen atom at the central position and are isoelectronic with the allyl anion. Although typically represented by closed-shell zwitterionic structures, diradical resonance structures can also be drawn for 1,3-dipoles. Generalized valence bond and configuration interaction calculations have shown that nitrilium, diazonium, and azomethine betaines have a small amount of diradical character, while carbonyl betaines and ozone have significant diradical character (~33% contribution).[19] However, diradical character does not necessitate a stepwise mechanism for the cycloadditions of these species.

There was a vigorous debate about whether 1,3-dipolar cycloadditions have concerted or stepwise mechanisms (Scheme 2).[20] On the basis of kinetic and stereochemical results, along with solvent and substituent effects, Huisgen proposed a concerted (although sometimes asynchronous) mechanism (Scheme 2a).[20a] On the basis of the same experimental evidence, Firestone postulated a stepwise diradical mechanism based on the lack of solvent effects and the lack of rate difference between alkene and alkyne dipolarophiles (Scheme 2b).[20b] In this two-stage mechanism, one σ-bond is formed preferentially and an unstable diradical intermediate is short-lived and cyclizes before C−C bond rotation, thus retaining stereochemistry. This is different than the stepwise mechanism involving a longer-lived anti-diradical (Scheme 2c).

Stereospecific cycloaddition of *para*-nitrobenzonitrile oxide to *cis*-1,2-dideuterioethylene and *trans*-1,2-dideuterioethylene later provided experimental proof of a concerted mechanism in a case where a putative diradical intermediate would be expected.[21] Multireference calculations performed by Robb and co-workers have also shown that the anti-diradical transition state for fulminic acid with acetylene is ~5 kcal/mol higher in energy than the concerted transition state.[22] Most current quantum chemical studies of 1,3-dipolar cycloadditions focus on concerted cycloadditions,[23,24] and there is no comprehensive comparison of stepwise versus concerted transition states using

(13) (a) Ess, D. H.; Jones, G. O.; Houk, K. H. *Adv. Synth. Catal.* **2006**, *348*, 2337. (b) Pross, A.; Shaik, S. S. *Acc. Chem. Res.* **1983**, *16*, 363–370.
(14) (a) Murdoch, J. R. *J. Am. Chem. Soc.* **1983**, *105*, 2660. (b) Murdoch, J. R. *J. Am. Chem. Soc.* **1983**, *105*, 2667. (c) Murdoch, J. R.; Morgan, Y. C. *J. Am. Chem. Soc.* **1984**, *106*, 4735. (d) Miller, A. R. *J. Am. Chem. Soc.* **1978**, *100*, 1984.
(15) Evans, M. G.; Polanyi, M. *Trans. Faraday Soc.* **1938**, *34*, 614.
(16) Koeppl, G. W.; Kresge, A. J. *J. Chem. Soc., Chem. Commun.* **1973**, 371.
(17) Marcus, R. A. *Pure Appl. Chem.* **1997**, *69*, 13.
(18) Ess, D. H.; Houk, K. N. *J. Am. Chem. Soc.* **2007**, *129*, 10646.
(19) (a) Walch, S. P.; Goddard, W. A., III. *J. Am. Chem. Soc.* **1975**, *97*, 5319. (b) Kahn, S. D.; Hehre, W. J.; Pople, J. A. *J. Am. Chem. Soc.* **1987**, *109*, 1871. (c) Hiberty, P. C.; Leforestier, C. *J. Am. Chem. Soc.* **1978**, *100*, 2012.
(20) (a) Huisgen, R. *J. Org. Chem.* **1968**, *33*, 2291. (b) Firestone, R. A. *J. Org. Chem.* **1968**, *33*, 2285.
(21) (a) Houk, K. N.; Firestone, R. A.; Munchausen, L. L.; Mueller, P. H.; Arison, B. H.; Garcia, L. A. *J. Am. Chem. Soc.* **1985**, *107*, 7227. (b) Houk, K. N.; González, J.; Li, Y. *Acc. Chem. Res.* **1995**, *28*, 81.
(22) (a) McDouall, J. J. W.; Robb, M. A.; Niazi, U.; Bernardi, F.; Schlegel, H. B. *J. Am. Chem. Soc.* **1987**, *109*, 4642. (b) Previous CI calculations actually favored a diradical mechanism: Hiberty, P. C.; Ohanessian, G.; Schlegel, H. B. *J. Am. Chem. Soc.* **1983**, *105*, 719.
(23) Nguyen, J. T.; Chandra, A. K.; Sakai, S.; Morokuma, K. *J. Org. Chem.* **1999**, 64.

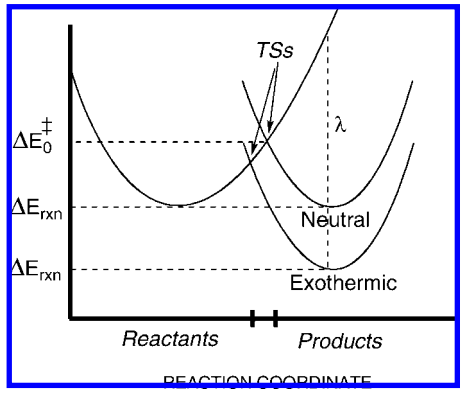

Figure 1. Marcus curve crossing showing a thermoneutral (intrinsic) and exothermic reaction.

modern computational methods. In this paper we compare concerted and stepwise (anti-diradical) transition state energies and geometries for six dipolar cycloadditions (dipoles **7**−**9**) with ethylene and acetylene using density functional theory.

Sustmann applied FMO theory to the reactivity of concerted 1,3-dipolar cycloadditions for substituted dipolarophiles.[8] He classified 1,3-dipolar cycloadditions depending on the importance of the two sets of frontier interactions. Three classes emerged on the basis of the dominating direction of charge-transfer, (1) dipole→dipolarophile, (2) dipolarophile→dipole, or (3) both. Class 1 reactions have the smallest energy separation between the 1,3-dipole highest occupied molecular orbital (HOMO) and the dipolarophile lowest unoccupied molecular orbital (LUMO). These reactions involve nucleophilic dipoles, such as diazomethane or other ylides, with high-lying HOMO orbitals and electrophilic dipolarophiles with low-lying LUMO orbitals. Electron-withdrawing groups on the dipolarophile accelerate reactions by lowering the LUMO orbital energy. Class 2 reactions have the opposite direction of charge-transfer. These dipolar cycloadditions have the smallest FMO gap between the dipole LUMO and the dipolarophile HOMO orbitals. These reactions involve electrophilic 1,3-dipoles, such as ozone. Dipolarophile electron-donating substituents enhance the rate of these reactions by diminishing the FMO gap. Class 3 involves nearly equivalent FMO gaps. This class is now referred to as ambiphilic. Such reactions give a parabolic plot of rates of reaction versus dipolarophile ionization potentials.[8] This arises because perturbation of ethylene frontier orbital energies decreases the frontier orbital gaps, either by lowering the LUMO or raising the HOMO of ethylene.

Thermodynamic models also provide a conceptual understanding of reactivity, and we have considered the possibility of applying such models to dipolar cycloadditions. Thermodynamic effects are typically conceptualized using a set of intersecting parabolic functions (one for reactants and one for products) along a reaction coordinate (Figure 1). This representation of a reaction pathway suggests that a transition state can be approximated as a point where the reactant bond dissociation transitions into the product bond formation. This leads to relationships between the reaction barriers and the relative energies and shapes of the two functions.

Marcus derived a quantitative treatment relating thermodynamic effects to the activation free energy for electron-transfer reactions (eq 1) based on the intersection of parabolic curves.[17] Here, reaction barriers are interpreted in terms of intrinsic barriers ($\Delta G_0^{\ddagger}$) for a reference thermoneutral ($\Delta G_{rxn} = 0$) reaction, and the energy of reaction, ΔG_{rxn} (Figure 1).[25] A simplified version of this equation, neglecting the second-order term (which is significant only when $|\Delta G_{rxn}| \gg \Delta G_0^{\ddagger}$) and using electronic energies instead of free energies is given in eq 2, and reduces down to the relationship, $\Delta\Delta E^{\ddagger} = 1/2\Delta\Delta E_{rxn}$, determined empirically for a set of related reactions by Dimroth,[26] Brønsted,[16] and Bell−Evans−Polanyi.[15] The intrinsic barrier, $\Delta G_0^{\ddagger}$ in eq 1, is defined by the curvature of the parabola and incorporates FMO interactions. The Marcus relationship for the transition state position, $x^{\ddagger}$, is given in eq 3; $x^{\ddagger}$ is proportional to the reaction free energy and inversely related to the intrinsic barrier.

$$\Delta G^{\ddagger} = \Delta G_0^{\ddagger} + \frac{1}{2}\Delta G_{rxn} + \frac{\Delta G_{rxn}^{\ 2}}{16\Delta G_0^{\ddagger}} \tag{1}$$

$$\Delta E^{\ddagger} = \Delta E_0^{\ddagger} + \frac{1}{2}\Delta E_{rxn} \tag{2}$$

$$x^{\ddagger} = \frac{1}{2} + \frac{\Delta G_{rxn}}{8\Delta G_0^{\ddagger}} \tag{3}$$

$$\Delta G^{\ddagger} = \frac{\lambda}{4}\left[1 + \frac{(\Delta G_{rxn})^2}{\lambda}\right] + \omega_r; \quad \lambda = \lambda_i + \lambda_o \tag{4}$$

A modified version of eq 1 is given in eq 4. Within the context of electron transfer, the so-called reorganization term, λ, is defined as the energy to convert the solvated reactant into the product while retaining reactant-like solvation. This is a sum of the solvation energy change (λ_o, outersphere) and the internal structure/vibronic level (λ_i, innersphere) changes. λ is the vertical excitation distance between the minimum point on the reactant parabola and the corresponding position on the product curve (or vice versa). In a molecular sense, this would be the energy of the product electronic configuration in the reactant geometry.

Computational Methodology

(U)B3LYP/6-31G(d) and compound quantum mechanical CBS-QB3 calculations were performed with the Gaussian 03 suite of programs.[27] For open-shell calculations, the spin-projection procedure of Yamaguchi and Houk[28] was applied using eqs 5 and 6, which approximately removes triplet contamination of the singlet wavefunction and the artificial lowering of the energy of the species due to a single determinate wavefunction.

$$E^{sp}{}_{singlet} = E_{singlet} + [\chi(E_{singlet} - E_{triplet})] \tag{5}$$

$$\chi = \frac{(^1\langle S^2\rangle / {}^3\langle S^2\rangle)}{1 - (^1\langle S^2\rangle / {}^3\langle S^2\rangle)} \tag{6}$$

The complete basis set (CBS) methods remove error in quantum mechanical calculations that arise from the truncation of basis sets. The CBS models extrapolate to an infinite basis set limit by using a N^{-1} asymptotic convergence of MP2 pair energies calculated from pair natural orbital expansions.[29] The CBS-QB3 method has a

(24) Su, M-D.; Liao, H-Y.; Chung, W-S.; Chu, S-Y. *J. Org. Chem.* **1999**, *64*, 6710.

(25) Marcus, R. A. *J. Chem. Phys.* **1956**, *24*, 966.
(26) Dimroth, O. *Angew. Chem.* **1933**, *46*, 571.
(27) Frisch, M. J.; et al. *Gaussian 03*, Revision C.02; Gaussian, Inc: Wallingford CT, 2004.
(28) Yamaguchi, K.; Takahara, Y.; Fueno, T.; Houk, K. N. *Theor. Chim. Acta* **1988**, *73*, 337.
(29) (a) Montgomery, J. A.; Frisch, M. J.; Ochterski, J. W.; Petersson, G. A. *J. Chem. Phys.* **2000**, *112*, 6532. (b) Montgomery, J. A.; Frisch, M. J.; Ochterski, J. W.; Petersson, G. A. *J. Chem. Phys.* **1999**, *110*, 2822. (c) Petersson, G. A.; Malick, D. K.; Wilson, W. G.; Ochterski, J. W.; Montgomery, J. A.; Frisch, M. J. *J. Chem. Phys.* **1998**, *109*, 10570.

Table 1. CBS-QB3 and B3LYP/6-31G(d) Activation and Reaction Enthalpies at 0 K for Reactions of Dipoles **1**−**9** with Ethylene and Acetylene (kcal/mol)[a]

	CBS-QB3		B3LYP	
dipole	$\Delta H^{\ddagger}$	ΔH_{rxn}	$\Delta H^{\ddagger}$	ΔH_{rxn}
1	27.9 (27.9)	−4.4 (−37.1)	25.1 (24.5)	−6.7 (−43.9)
2	20.3 (20.1)	−19.7 (−61.5)	19.5 (18.6)	−20.2 (−64.9)
3	14.6 (15.2)	−31.7 (−49.0)	16.6 (16.4)	−30.6 (−51.4)
4	13.0 (14.1)	−39.3 (−74.0)	13.3 (13.7)	−39.8 (−79.0)
5	7.2 (8.5)	−57.4 (−100.3)	8.7 (9.1)	−55.6 (−102.0)
6	5.9 (7.4)	−68.0 (−86.7)	8.8 (10.6)	−65.1 (−87.6)
7	13.8 (14.0)	−28.8 (−43.9)	13.7 (13.0)	−28.7 (−48.1)
8	7.8 (7.6)	−44.2 (−59.5)	9.7 (8.7)	−42.5 (−62.0)
9	0.9 (1.5)	−62.7 (−76.9)	3.5 (3.6)	−61.2 (−79.2)

[a] Acetylene values are given in parentheses.

maximum error of 2.8 kcal/mol for the G2 test set, and average and mean absolute errors of 0.20 and 0.98 kcal/mol. On a B3LYP/6-311G(d,p) geometry, the following energy corrections are used to give a final CBS-QB3 energy ($E^{CBS\text{-}QB3}$):

$$E^{CBS\text{-}QB3}(H_{(0K)}) = E(\text{MP2/6-311+G(2df, 2p)} - \text{CBSB7}) + E(\text{MP2 CBS extrapolation}) + E(\text{MP4(SDQ)/6-31+G(d, p)} - \text{CBSB4}) - E(\text{MP2/6-31G+(d, p)} - \text{CBSB4}) + E(\text{CCSD(T)/6-31+G}^{\dagger}) - E(\text{MP4(SDQ)/6-31+G}^{\dagger}) + E_{ZPE}(\text{B3LYP/6-311G(d, p)}) + E(\text{int}) + E(\text{empirical})$$

Reported HOMO and LUMO energies and gaps were calculated using the RHF/6-311++G(2d,p) level of theory on B3LYP/6-31G(d) geometries, because Kohn−Sham orbitals often provide poor estimates for ionization potentials of simple organic molecules and the medium size 6-31G(d) basis set often gives inaccurate unoccupied orbital eigenvalues.[30]

Results and Discussion

The CBS-QB3 method was used initially to compute the activation and reaction enthalpies for 18 1,3-dipolar cycloadditions. Nine 1,3-dipoles (**1**−**9**), from the diazonium, nitrilium, and azomethine betaines classes, and their reactions with ethylene and acetylene were explored. This set of 1,3-dipolar cycloadditions encompasses reactions of nucleophilic, electrophilic, and ambiphilic dipoles. The CBS-QB3 (and for comparison, B3LYP) activation and reaction enthalpies at 0 K are listed in Table 1 (estimated average error ±1 kcal/mol).[18,31] A wider variety of dipolarophiles is discussed later in this paper.

The CBS-QB3 activation barriers in Table 1 are graphically displayed in Figure 2, classified into oxides, imines, and ylides. This graph shows some expected trends based on FMO theory and several surprising quantitative results. First, there is a smooth decrease in barrier height from oxides to imines to ylides, amounting to a 6 ± 1 kcal/mol lowering of the barrier for oxide to imine and imine to ylide, except for the nitrilium ylide. While this is well known to be the order of reactivity, there is a remarkable consistency in the slope of these lines for different 1,3-dipoles, with only formonitrile ylide **6** deviating from the pattern. The barrier for nitrilium ylide cycloaddition to ethylene and acetylene is about 6 kcal/mol too high compared to azomethine ylide. Second, the nitrilium and azomethine betaine classes, which have the same X−Y−Z heteroatoms ($HC{\equiv}N^{+}{-}Z^{-}$/$H_2C{=}N^{+}H{-}Z^{-}$), have almost identical barrier heights. Third, ethylene and acetylene barrier differences are within 1.5 kcal/mol for a given type of 1,3-dipole.

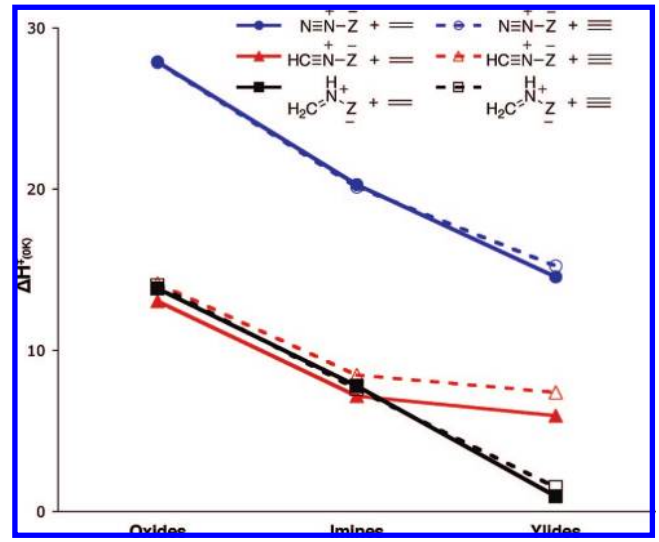

Figure 2. Graphical display of CBS-QB3 $\Delta H^{\ddagger}_{0K}$ versus dipole heteroatom Z = O (oxides), NH (imines), CH_2 (ylides), for cycloadditions with ethylene (solid lines) and acetylene (dotted lines).

Equivalent ethylene and acetylene barriers were unexpected on the basis of FMO interactions, because the FMO energies from ionization potential and electron affinity values are −10.5 and 1.5 eV for ethylene and −11.5 and 2.5 eV for acetylene.[32] Nearly identical ethylene and acetylene barriers were also surprising on the basis of the very different reaction exothermicities (ΔH_{rxn}) listed in Table 1; formation of aromatic products from acetylene is not accompanied by unusually low barriers for these highly thermodynamically advantageous reactions. The four 1,3-dipoles (**1**, **2**, **4**, and **5**) capable of forming aromatic cycloadducts with acetylene have an average $\Delta\Delta H_{rxn}$ of 38 kcal/mol between ethylene and acetylene reactions. The remaining dipoles, **3**, **6**, and **7**−**9**, which are incapable of forming aromatic cycloadducts, also have a significant average $\Delta\Delta H_{rxn}$ (16 kcal/mol) between ethylene and acetylene reactions.

While experimental data are not available for ethylene and acetylene,[33] Huisgen observed the similar reactivity of a few substituted dipoles with related alkene and alkyne dipolarophiles. Table 2 gives the experimental ratio of rates observed for dipolar cycloadditions comparing styrene/phenylacetylene and acrylic/propiolic esters with phenyl-substituted versions of dipoles **2**, **3**, **4**, and **5**. Three of these reactions form aromatic 1,2,3-triazoles, isoxazoles, and pyrazoles upon addition to phenylacetylene and propiolic ester, yet there is only a rate difference of ∼10 fold for reactions with diphenylnitrile imine and benzonitrile oxide and essentially equal reactivity with diphenyldiazomethane and phenyl azide.

Figure 3 shows a test of the reactivity/thermochemistry relationship, $\Delta\Delta E^{\ddagger} = 1/2\Delta\Delta E_{rxn}$. Obviously, there is no simple

(30) (a) Politzer, P.; Abu-Awwad, F. *Theor. Chem. Acc.* **1998**, *99*, 83. (b) Kar, T.; Ángyán, J. G.; Sannigrahi, A. B. *J. Phys. Chem. A* **2000**, *104*, 9953. (c) Zhang, G.; Musgrave, C. B. *J. Phys. Chem. A* **2007**, *111*, 1554.
(31) Ess, D. H.; Houk, K. N. *J. Phys. Chem. A* **2005**, *109*, 9542.
(32) Values taken from the National Institute of Standards and Technology (NIST) Chemistry Webbook (NIST Standard Reference Database Number 69, June 2005 Release).
(33) The only parent reaction studied experimentally is that of diazomethane cycloaddition to ethylene in DMF. See: (a) Geittner, J.; Huisgen, R.; Sustmann, R. *Tetrahedron Lett.* **1977**, *10*, 881. (b) Geittner, J.; Huisgen, R.; Reissig, H.-U. *Heterocycles* **1978**, *11*, 109.

Table 2. Experimental Ratios of Rates for 1,3-Dipolar Cycloadditions with Double and Triple C−C Bonds[a]

1,3-Dipole	Ph (Ph)	COOR (COOR)
Diphenyl(nitrile imine) (80° C)	12.0	8.5
Benzonitrile oxide (20° C)	9.2	5.7
Diphenyldiazomethane (40° C)	1.2	0.7
Phenyl azide (25° C)	1.4	1.0

[a] Values taken from ref 6.

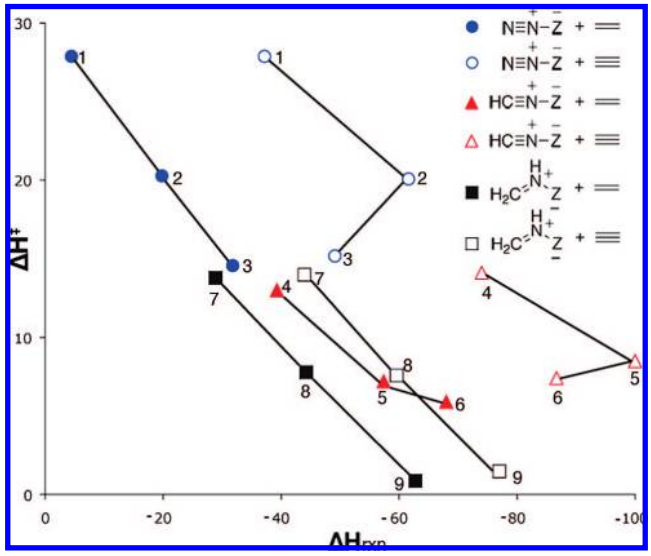

Figure 3. Plot of CBS-QB3 activation enthalpies at 0 K ($\Delta H^{\ddagger}_{0K}$) versus reaction enthalpies at 0 K ΔH_{rxn} (kcal/mol). Solid lines connect (left to right) oxide, imine, and ylide in each series.

relationship for all dipoles, although in general, a decrease in barrier height is associated with more exothermic reactions. Reactions of dipoles **1**−**3** (diazonium) with ethylene, and **7**−**9** (azomethine) with ethylene and acetylene follow the $\Delta\Delta E^{\ddagger} = 1/2\Delta\Delta E_{rxn}$ generalization. However, this relationship does not hold for reactions of dipoles **4**−**6** (nitrilium) with ethylene nor **1**−**3** and **4**−**6** with acetylene. The change from aromatic to nonaromatic cycloadducts causes these series of reactions to deviate dramatically from an expected linear relationship. Also, comparison of ethylene and acetylene points lie at very different positions on this graph. We conclude that there is no general relationship of the Dimroth−Brønsted−Marcus type for these bimolecular 1,3-dipolar cycloaddition reactions, and the excellent relationships of this type for diazonium betaines with ethylene and of azomethine betaines with both ethylene and acetylene might reflect the correlation of reaction thermodynamics to some other more fundamental quantity related to the transition state itself (see later). Also, within the context of the curve crossing model of Pross and Shaik,[34] identical ethylene and acetylene barriers were also surprising because the ground-state singlet−triplet gaps of ethylene and acetylene differ by ~17 kcal/mol,[35] which should lead to substantially different reactivity.

Transition Structures. Figure 4 shows overlays of the CBS-QB3 transition states for reactions of **1**−**9** with ethylene and acetylene. The ground-state geometry of each 1,3-dipole is also shown above each of the transition states. These structures are concerted and nearly synchronous. Ethylene and acetylene transition states are so similar that only the positions of the hydrogen atoms reveal that each picture actually represents a superposition of two transition structures.

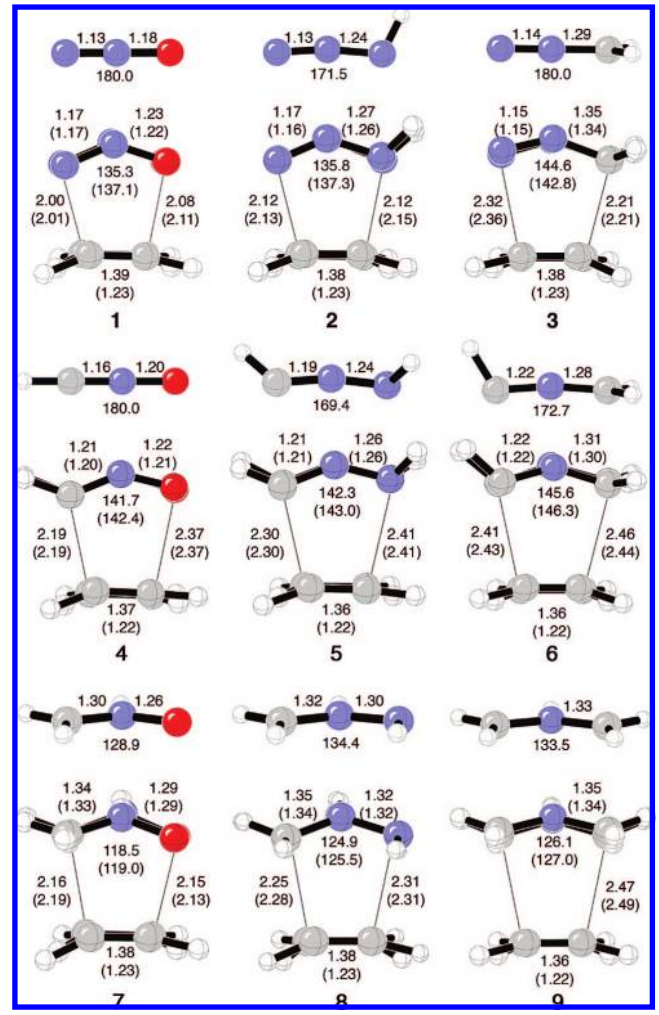

Figure 4. Overlay of CBS-QB3 (B3LYP/6-311G(d,p)) transition structure geometries of ethylene and acetylene reactions with 1,3-dipoles **1**−**9**. The structure of each 1,3-dipole is shown above the transition structures. Bond lengths are reported in Å. Values in parenthesis are for acetylene reactions. Reprinted with permission from ref 18.

There is a tendency toward early and late transition states in these structures. This trend is related to the barrier heights, not ΔH_{rxn}, as typically invoked in the Hammond postulate.[36] For each 1,3-dipole series (Z = O, NH, CH_2), there is a shift from

(34) The valence-bond configuration mixing treatment of Pross and Shaik describes reaction pathways (including the transition state) based on the extent of mixing of ground and excited state configurations and focuses on the specific bonds that are made and broken and their relative configurations. In this model the barrier is a result from an avoided crossing of two spin configuration wavefunctions. For 1,3-dipolar cycloadditions this would involve the avoided crossing of the singlet ground state of the 1,3-dipole and dipolarophile leading to the cycloadduct in a triplet excited state and the reactants in the excited state triplet state leading to the singlet product ground state. The transition state is then a function of the avoided curve crossing of the singlet and triplet states for the forming σ-bonds and is typically correlated with the singlet−triplet energy gap (ΔE_{ST}) of the reactants; a lower ΔE_{ST} value for the reactants gives a lower barrier, earlier transition state, and greater exothermic reaction energy. See refs 23, 24, and the following: (a) Liao, H-Y.; Su, M-D.; Chung, W-S.; Chu, S-Y. *Int. J. Quant. Chem.* **2001**, *83*, 318. (b) Sakai, S.; Nguyen, M. T. *J. Phys. Chem. A* **2004**, *108*, 9169. (c) Sakai, S.; Nguyen, M. T. *J. Phys. Chem. A* **2000**, *104*, 922.

(35) (a) Nguyen, M. T.; Matus, M. H.; Lester, W. A., Jr.; Dixon, D. A. *J. Phys. Chem. A* **2008**, *112*, 2082. (b) Le, H. T.; Flock, M.; Nguyen, M. T. *J. Chem. Phys.* **2000**, *112*, 7008. (c) Van Veen, E. H. *Chem. Phys. Lett.* **1976**, *41*, 540.

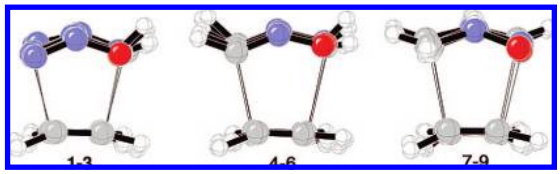

Figure 5. Overlay of all diazonium (**1**−**3**), nitrilium (**4**−**6**), and azomethine (**7**−**9**) CBS-QB3 transition structures with ethylene and acetylene.

Table 3. Transition State Angles

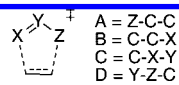

Dipole		XYZ	A	B	C	D
1	C_2H_4	135	100	104	101	98
	C_2H_2	137	101	106	99	95
2	C_2H_4	136	101	103	100	99
	C_2H_2	137	102	106	98	95
3	C_2H_4	145	105	100	96	95
	C_2H_2	143	108	101	93	92
4	C_2H_4	124	101	103	101	93
	C_2H_2	124	100	107	98	91
5	C_2H_4	124	101	103	99	93
	C_2H_2	124	101	106	98	91
6	C_2H_4	146	103	102	96	92
	C_2H_2	146	106	102	93	91
7	C_2H_4	119	102	103	95	93
	C_2H_2	119	103	105	92	92
8	C_2H_4	125	102	103	95	93
	C_2H_2	125	104	102	92	94
9	C_2H_4	126	102	102	92	92
	C_2H_2	127	104	104	90	90

late to early transition state as the activation barrier drops. The average of the forming bond lengths increases by 0.1−0.3 Å. The C−C bond lengths of the dipolarophiles are only 0.03−0.06 longer in the transition state than in the reactant, and only change by 0.01−0.02 Å across each series from late to early. Similarly, the heavy atom bond lengths of the dipoles change by only 0.01−0.06 Å from reactants to the transition states. Most notably, each transition state involves significant bending of the 1,3-dipole angles from their linear or planar ground-state geometries to a product-like bending angle. The out-of-plane angle changes from the ground state to the transition state range from 26° to 45° for dipoles **1**−**6**. The degree of angle change is smaller for ylides, corresponding to earlier transition states. Nevertheless, in spite of these differences, all 18 transition states shown in Figure 4 are remarkably similar; the main feature is bending of the 1,3-dipole to achieve overlap of the π orbitals at the termini with those of the dipolarophiles. There is only ∼1° difference in dipole transition state angle between ethylene and acetylene geometries. Figure 5 shows overlays of all transition structures for each class of dipoles (diazonium, nitrilium, and azomethine) and highlights the similarity of all transition states, especially within each class of betaines. The heavy atom angles are listed in Table 3. For angles *A* and *B*, they range between 100° and 105° for ethylene transition states, and 100° and 108° for acetylene geometries. Angles *C* and *D* have slightly larger ranges, 92−100° for ethylene and 90−99° for acetylene. The narrow range of heavy atom angles further illustrates the similarities of the transition structures, which differ only by a slight change from late to early in the forming partial bond lengths.

The transition states for reactions **7**−**9** are consistent with the Huisgen concerted model for allylic dipoles. However, for transition states with dipoles **1**−**6**, all heavy atoms are in the plane of the forming ring. This means that for transition states of dipoles **1**, **2**, **4**, and **5** with acetylene, the out-of-plane π-systems have the possibility to interact but do not lead to extra transition state stabilization because the transition states have product-like-geometries only with respect to bending of the 1,3-dipole.[37] The alkene and alkyne C−C bond lengths are negligibly disrupted, increasing by <0.05 Å. The dipole bond lengths increase only by an average of 0.03 Å.

Concerted vs Stepwise Mechanisms. The B3LYP stepwise transition states and intermediates for addition of dipoles **7**−**9** to ethylene and acetylene are shown in Figure 6. No transition state for diradical formation could be located by UB3LYP for most of the addition of dipoles **1**−**6** due to a lack of radical stabilizing groups.[38] Table 4 gives the UB3LYP and spin-projected (SP) UB3LYP activation barriers. Even after spin projection, the energy for concerted cycloadditions are below stepwise additions. The barrier difference between concerted and stepwise addition, $\Delta\Delta H^{\ddagger}_{(S-C)}$, ranges from 1.2 to 8.1 kcal/mol. $\Delta\Delta H^{\ddagger}_{(S-C)}$ increases along the azomethine series from oxides to ylides due to the lowering of the dipole singlet−triplet gap.

Stepwise addition proceeds through an anti-diradical geometry between the dipole and the alkene or alkyne. The C−C−C−Z dihedral angle ranges from 170° to 175° for ethylene reactions, and 144° to 156° for acetylene. In these transition states, the dipole is less bent than in the concerted transition states but the methylene (H_2C) group is significantly pyramidalized. For ethylene reactions, pyramidalization only occurs on the carbon involved in bond formation. The other alkene carbon center remains unpyramidalized. For acetylene reactions, the HCC angle bends significantly to allow for bond formation. The second HCC angle for the nonbond forming carbon bends to 159° ± 4°. The angle increases to an average of 137° ± 1° in the intermediates.

The large difference in stepwise transition state geometries for ethylene versus acetylene addition leads to a substantial difference in activation barriers.[40] The average $\Delta\Delta H^{\ddagger}$ between ethylene and acetylene reactions is 4.6 kcal/mol (3.7 kcal/mol for SP values). Alkyne addition is easier due to the (relatively) easier bending of acetylene versus ethylene for single-bond nucleophilic addition.[41] When concerted two-bond transition states occur, both HCC angles of acetylene bend in the same direction, while for stepwise additions, the two HCC angles bend in opposite directions leading to extra stabilization for alkyne reactions. This study, as well as a variety of others in the literature,[23,24] shows that the concerted pathways are favored over the stepwise, as described by Huisgen. The Firestone

(36) (a) Hammond, G. S. *J. Am. Chem. Soc.* **1955**, *77*, 334. (b) Evans, M. G.; Polanyi, M. *Trans. Faraday Soc.* **1938**, *34*, 11.

(37) Poppinger, D. *J. Am. Chem. Soc.* **1975**, *97*, 7486.

(38) For dipoles **1**−**6**, only the stepwise transition state for HCNO + acetylene was located with UB3LYP.

(39) The B3LYP S^2 value of **9-S-TS-A** is 0.000621. The origin of this unexpected lack of spin-contamination in the transition state remains unknown. The transition state has a single negative frequency corresponding to C−C bond formation, and IRC calculations connect it with separated reactants and **9-S-A**, which has an S^2 value of 0.84, indicating significant singlet−triplet mixing. Several other DFT methods (such as mpwpw91) were examined and all give similarly small S^2 values.

(40) (a) Valentin, C. D.; Freccero, M.; Gandolfi, R.; Rastelli, A. *J. Org. Chem.* **2000**, *65*, 6112.

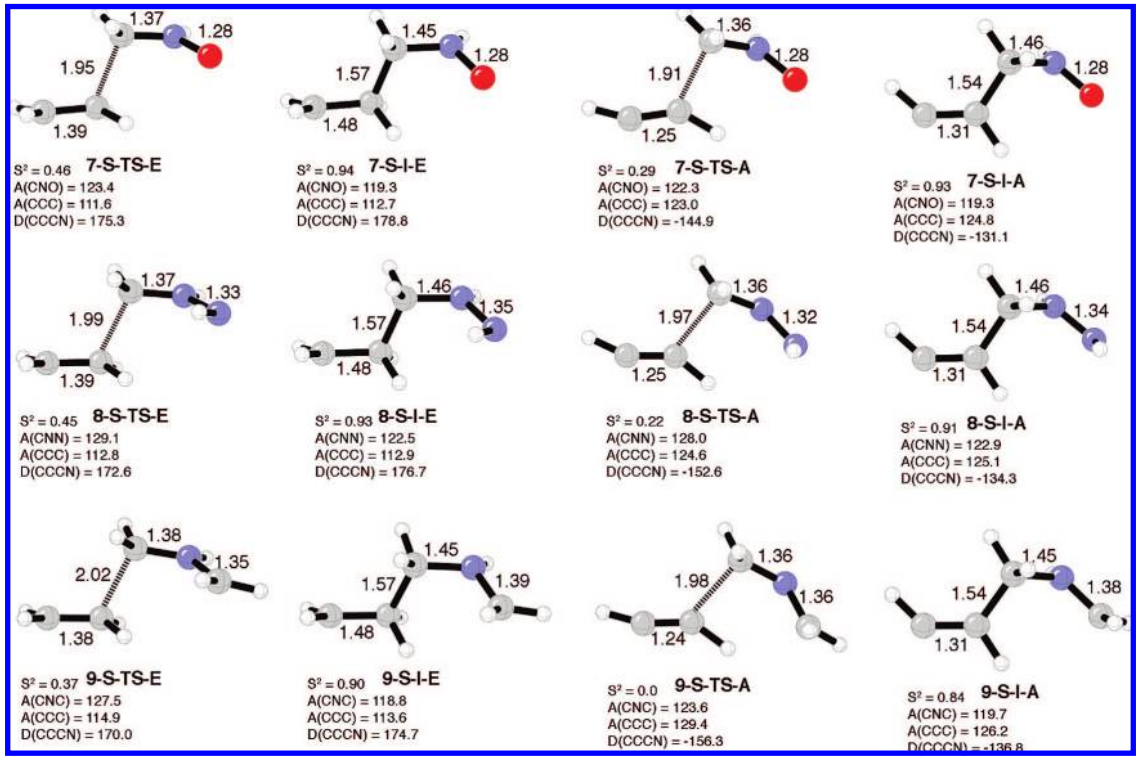

Figure 6. UB3LYP/6-31G(d) stepwise (**S**) transition states (**TS**) and intermediates (**I**) for reactions of dipoles **7**−**9** with ethylene (**E**) and acetylene (**A**). Spin-contamination (S^2) values are also given.[39]

Table 4. UB3LYP/6-31G(d) and Spin-Projected (SP) UB3LYP Activation and Reaction Enthalpies for Stepwise Addition of Dipoles **7**−**9** to Ethylene and Acetylene[a]

		C_2H_4		C_2H_2	
			SP		SP
7-S-TS	$\Delta H^{\ddagger}$	21.6	16.2	18.1	14.2
7-S-I	ΔH	13.0	10.9	8.1	5.5
	$\Delta\Delta H^{\ddagger}_{(S-C)}$		2.5		1.2
8-S-TS	$\Delta H^{\ddagger}$	19.4	14.4	16.0	13.1
8-S-I	ΔH	9.9	7.9	4.6	1.8
	$\Delta\Delta H^{\ddagger}_{(S-C)}$		4.7		4.4
9-S-TS	$\Delta H^{\ddagger}$	15.7	11.6	11.2	11.2
9-S-I	ΔH	5.5	2.6	−0.7	−4.1
	$\Delta\Delta H^{\ddagger}_{(S-C)}$		8.1		7.6

[a] Enthalpy difference between stepwise and concerted addition is also given ($\Delta\Delta H^{\ddagger}_{(S-C)}$). Values are reported in kcal/mol.

stepwise mechanism is known only for highly substituted dipoles and dipolarophiles.[42]

Relationship of Distortion Energy to Activation Energy. The activation energy ($\Delta E^{\ddagger}$) for bimolecular reactions can be dissected into the distortion energy ($\Delta E_d^{\ddagger}$) and the energy of interaction ($\Delta E_i^{\ddagger}$) between distorted fragments. The distortion energy (or deformation energy as it is called by Morokuma[43] and activation strain by Bickelhaupt[44]) is the energy required to distort the 1,3-dipole and the dipolarophile into the geometries they have in the transition state without allowing interaction between the addends.[45] The activation energy is then $\Delta E^{\ddagger} = \Delta E_d^{\ddagger} + \Delta E_i^{\ddagger}$,[46] where E can be electronic, enthalpic, or free energy. Table 5 lists the B3LYP/6-31G(d) activation, transition

(41) (a) Strozier, R. W.; Caramella, P.; Houk, K. N. *J. Am. Chem. Soc.* **1979**, *101*, 1340. (b) Houk, K. N.; Rondan, N. G.; Schleyer, P.v-R.; Kaufmann, E.; Clark, T. *J. Am. Chem. Soc.* **1985**, *107*, 2821. (c) Rondan, N. G.; Domelsmith, L. N.; Houk, K. N.; Bowne, A. T.; Levin, R. H. *Tetrahedron Lett.* **1979**, *35*, 3237.

(42) (a) Huisgen, R.; Mloston, G.; Langhals, E. *J. Am. Chem. Soc.* **1986**, *108*, 6401. (b) Huisgen, R.; Mloston, G.; Langhals, E. *J. Org. Chem.* **1986**, *51*, 4085. (c) Weber, A.; Sauer, J. *Tetrahedron Lett.* **1998**, *39*, 807. (d) Vivanco, S.; Lecea, B.; Arrieta, A.; Prieto, P.; Morao, I.; Linden, A.; Cossio, F. P. *J. Am. Chem. Soc.* **2000**, *122*, 6078.

(43) (a) Kitaura, K.; Morokuma, K. *Int. J. Quant. Chem.* **1976**, *10*, 325. (b) Nagase, S.; Morokuma, K. *J. Am. Chem. Soc.* **1978**, *100*, 1666. (c) Houk, K. N.; Gandour, R. W.; Strozier, R. W.; Rondan, N. G.; Paquette, L. A. *J. Am. Chem. Soc.* **1979**, *101*, 6797. (d) Froese, R. D. J.; Coxon, J. M.; West, S. C.; Morokuma, K. *J. Org. Chem.* **1997**, *62*, 6991. (e) Koga, N.; Ozawa, T.; Morokuma, K. *J. Phys. Org. Chem.* **1990**, *3*, 519. (f) Coxen, J. M.; Grice, S. T.; Maclagan, R. G. A. R.; McDonald, D. Q. *J. Org. Chem.* **1990**, *55*, 3804. (g) Coxon, J. M.; Rroese, R. D. J.; Ganguly, B.; Marchand, A. P.; Morokuma, K. *J. Synnlett* **1999**, *11*, 1681. (h) Avalos, M.; Babiano, R.; Bravo, J. L.; Cintas, P.; Jiménez, J.; Palacios, J.; Silva, M. A. *J. Org. Chem.* **2000**, *65*, 6613. (i) Geetha, K.; Dinadayalane, T. C.; Sastry, G. N. *J. Phys. Org. Chem.* **2003**, *16*, 298. (j) Manoharan, M.; Venuvanalingam, P. *J. Chem. Soc., Perkin Trans. 2* **1997**, 1799. (k) Kavitha, K.; Manoharan, M.; Venuvanalingam, P. *J. Org. Chem.* **2005**, *70*, 2528. (l) Kavitha, K.; Venuvanalingam, P. *Int. J. Quant. Chem.* **2005**, *104*, 67. (m) Blowers, P.; Ford, L.; Masel, R. *J. Phys. Chem. A* **1998**, *102*, 9267.

(44) (a) Bickelhaupt, F. M. *J. Comput. Chem.* **1999**, *20*, 114. (b) Velde, G. T.; Bickelhaupt, F. M.; Baerends, E. J.; Guerra, C. F.; Gisbergen, S. J. A. V.; Snijders, J. G.; Ziegler, T. *J. Comput. Chem.* **2001**, *22*, 931. (c) Diefenbach, A.; Bickelhaupt, F. M. *J. Chem. Phys.* **2001**, *115*, 4030. (d) Diefenbach, A.; Bickelhaupt, F. M. *J. Phys. Chem. A* **2004**, *108*, 8460. (e) Diefenbach, A.; Bickelhaupt, F. M. *J. Organomet. Chem.* **2005**, *690*, 2191. (f) Diefenbach, A.; de Jong, G. T.; Bickelhaupt, F. M. *Mol. Phys.* **2005**, *103*, 995. (g) Diefenbach, A.; de Jong, G. T.; Bickelhaupt, F. M. *J. Chem. Theory Comput.* **2005**, *1*, 286. (h) Stralen, J. N. P.v.; Bickelhaupt, F. M. *Organometallics* **2006**, *25*, 4260. (i) de Jong, G. T.; Visser, R.; Bickelhaupt, F. M. *J. Organomet. Chem.* **2006**, *691*, 4341. (j) de Jong, G. T.; Bickelhaupt, F. M. *Chem. Phys. Chem.* **2007**, *8*, 1170. (k) de Jong, G. T.; Bickelhaupt, F. M. *J. Chem. Theory Comput.* **2007**, *3*, 514.

(45) Ziegler and Rauk have considered distortion energy as apart of their extended transition state method: (a) Ziegler, T.; Rauk, A. *Theor. Chim. Acta* **1977**, *46*, 1. (b) Ziegler, T.; Rauk, A. *Inorg. Chem.* **1979**, *18*, 1755. (c) Bickelhaupt, F. M.; Ziegler, T.; Schleyer, P. v. R. *Organometallics* **1995**, *14*, 2288.

Table 5. B3LYP/6-31G(d) Activation, Distortion and Interaction Energies for Reaction of Dipoles **1**−**9** with Ethylene (ENE) and Acetylene (YNE)[a]

	$\Delta E^{\ddagger}$		$\Delta E_d^{\ddagger}$		$\Delta E_i^{\ddagger}$	
dipole	ENE	YNE	ENE	YNE	ENE	YNE
1	23.5	23.3	37.3	34.7	−13.8	−11.4
2	17.2	16.9	26.4	25.0	−9.2	−8.1
3	14.3	14.5	21.6	21.9	−7.3	−7.4
4	11.4	12.1	18.3	18.4	−6.9	−6.3
5	6.9	7.8	12.4	13.1	−5.5	−5.3
6	6.9	8.1	12.8	14.4	−5.9	−6.3
7	11.4	11.1	18.3	18.4	−6.9	−7.3
8	7.3	6.8	15.3	15.4	−8.0	−8.6
9	1.2	1.9	6.8	7.5	−5.6	−5.6

[a] Values reported in kcal/mol.

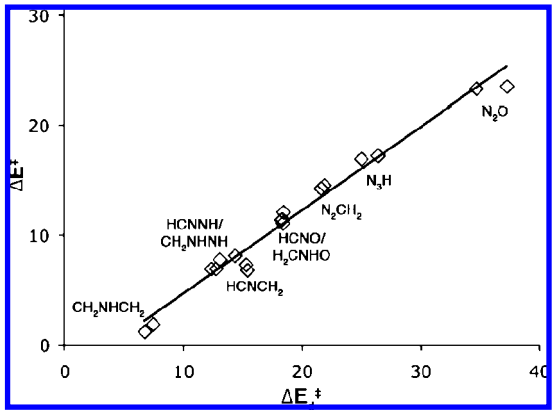

Figure 7. Plot of B3LYP/6-31G(d) total distortion energies versus activation energies for reactions **1**−**9** with ethylene and acetylene (kcal/mol). $\Delta E^{\ddagger} = 0.75\Delta E_d^{\ddagger} - 2.9$; $R^2 = 0.97$.

state distortion, and transition state interaction energies, for reactions of dipoles **1**−**9** with ethylene and acetylene. This more economical method predicts barriers within a mean absolute deviation of 1.5 kcal/mol compared to CBS-QB3.[47] Figure 7 is a plot of $\Delta E_d^{\ddagger}$ versus $\Delta E^{\ddagger}$ for the 18 reactions studied and gives a relationship of $\Delta E^{\ddagger} = 0.75\Delta E_d^{\ddagger} - 2.9$ kcal/mol; $R^2 = 0.97$.[48] This linear correlation was unexpected, since many reactions give no general correlation between rates and distortion energies, and indicates that a large barrier is the result of a large distortion energy at the transition state. To test the generality of this relationship, $\Delta E^{\ddagger}$ and $\Delta E_d^{\ddagger}$ for reactions of several substituted dipoles, including methyl, trifluoromethyl, dicyano, and amido were computed (Table 6). Highly electron-withdrawing groups substituted on the methylene ylide terminal of dipoles **3** and **6** simultaneously increases the barrier height and transition state distortion energy. Table 6 also gives the distortion and interaction energies for several other important 1,3-dipoles including carbonyl oxide (CH_2OO), ozone (O_3), and HNO_2 which span a wide range of activation barriers (−3 to +31 kcal/mol). The two other parent carbonyl betaines (CH_2ONH and CH_2OCH_2) have barrierless cycloadditions with ethylene and acetylene. All activation and distortion energies for the substituted 1,3-dipole

Table 6. B3LYP/6-31G(d) $\Delta E^{\ddagger}$, $\Delta E_d^{\ddagger}$, and $\Delta E_i^{\ddagger}$ for Cycloadditions of Substituted 1,3-Dipoles with Ethylene and Other Important 1,3-Dipoles (kcal/mol)

1,3-dipole	dipolarophile	$\Delta E^{\ddagger}$	$\Delta E_d^{\ddagger}$	$\Delta E_i^{\ddagger}$
$N_2CH(CONH_2)$	C_2H_4	17.5	26.6	−9.1
$N_2CH(CN)_2$	C_2H_4	16.9	28.8	−11.7
$N_2CH(CF_3)$	C_2H_4	14.1	22.6	−8.5
$N_2CH(CH_3)$	C_2H_4	13.5	20.8	−7.3
$HCNC(CN)_2$	C_2H_4	5.3	11.8	−6.5
CH_2OO	C_2H_4	−2.0	3.5	−5.5
	C_2H_2	−0.9	5.5	−6.4
O_3	C_2H_4	−3.1[49]	2.5	−5.6
	C_2H_2	−0.1	5.0	−5.1
HNO_2	C_2H_4	31.3	25.0	−6.3

reactions and these other important 1,3-dipoles fit on the same straight line with the 18 reactions already studied.

Although the barrier heights are not a simple function of reaction energy,[50] they are remarkably correlated with the distortion energies. Figure 8 illustrates how the distortion, interaction, and activation energies are related. The distortion energy involves simultaneous geometric and electronic change and is different from Marcus's reorganization energy, λ, which relates to the energy of the electronic structure of the product in the reactant geometry, rather than the transition state geometry, where our distortion energy is measured.[17] Distortion energy is typically neglected in qualitative FMO treatments and is independent of thermodynamic effects.

The concerted 1,3-dipolar cycloaddition transition states occur at the geometry at which the overlap between the orbitals of the termini of the cycloaddends is largest, and the FMO gaps have been narrowed sufficiently so that stabilizing charge-transfer interactions overcome destabilizing distortions. The derivatives of distortion and interaction energy are equal and opposite at the transition state ($\delta\Delta E_d = -\delta\Delta E_i$), and further motion leads directly to the cycloadduct with a decrease in energy. To achieve this transition state geometry requires significant distortion, and almost product-like geometries, of the dipole (see Figure 4). The energy of distortion toward a product-like structure is of course related to the dipole ground-state stability, that is, the equilibrium dipole electronic structure; stable low-energy dipoles are hard to distort, while high-energy 1,3-dipoles are easy to distort.

The majority of the transition state distortion energy (∼80%) arises from deformation of the 1,3-dipole due to angle change to achieve a product-like structure to narrow the FMO gaps and increase intermolecular orbital overlap. Table 7 lists the components of the dipole distortion energy resulting angle (X−Y−Z) and bond length (X−Y + Y−Z) distortions. The energy required for this angle change is the major distortion

(46) In a unimolecular reaction, $\Delta E^{\ddagger} = \Delta E_d^{\ddagger}$.

(47) Jones, G. O.; Ess, D. H.; Houk, K. N. *Helv. Chim. Acta* **2005**, *88*, 1702.

(48) If the distortion energy of each fragment (dipole and dipolarophile) is computed in the presence of each other, i.e., allowing polarization only, the linear relationship becomes $\Delta E^{\ddagger} = 0.86\Delta E_d^{\ddagger}$, with the intercept equal to zero. Ess, D. H.; Khaliullin, R. Z.; Head-Gordon, M.; Houk, K. N. Manuscript in preparation.

(49) For a definitive study on the activation barriers for the dipolar cycloadditions of ozone with ethylene and acetylene, see: Wheeler, S. E.; Ess, D. H.; Houk, K. N. *J. Phys. Chem. A* **2008**, *112*, 1798.

(50) (a) There are two possibilities for the above kinetic and thermodynamic results to be "fitted" to Marcus theory. (1) A compensation effect, where the parabola curvature (change in $\lambda/4$) exactly cancels any increase in reaction energy or (2) the barrier trends are only due to changes in Marcus's work function, ω_r. Yates has proposed an alternative form of the Marcus equation that includes an eccentricity or asymmetry variable (ranging from 0 to 1) in front of the intrinsic barrier term. See: Yates, K. *J. Am. Chem. Soc.* **1986**, *108*, 6511. Point 2 was suggested by personal communication with R. Marcus. (b) When reactant and product parabola curvature are nearly equal, there is typically much better correlation between activation barriers and reaction energies. See for example: Alabugin, I. V.; Manoharan, M.; Breiner, B.; Lewis, F. D. *J. Am. Chem. Soc.* **2003**, *125*, 9329.

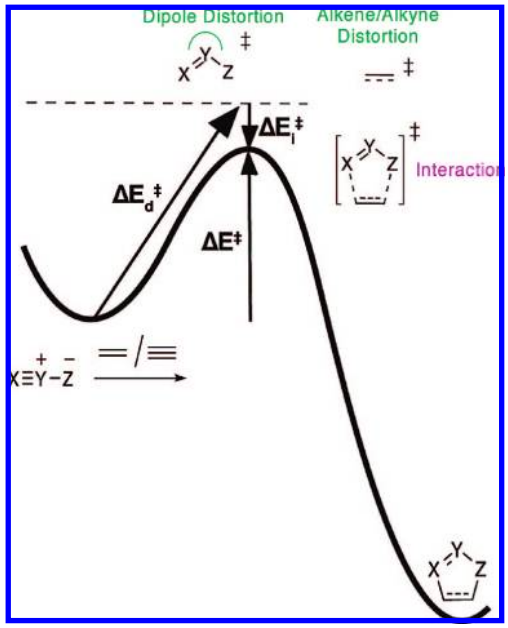

Figure 8. Relationship between activation, distortion, and interaction energies.

Table 7. B3LYP/6-31G(d) Ethylene (ENE) and Acetylene (YNE) Transition State Distortion Energies, and Dipole Angle (XYZ) and Bond Distortion Energies for Reactions of **1**−**6** with Ethylene (kcal/mol)

dipole	ENE	YNE	$\Delta E_d^‡$ angle (XYZ)	bond (X−Y + Y−Z)
1	6.1	6.5	27.1	4.1
2	5.4	6.3	18.2	2.8
3	4.7	6.8	12.5	4.3
4	2.9	4.0	12.5	2.9
5	2.5	3.8	8.9	0.7
6	2.7	4.9	7.6	0.6
7	5.7	7.5		
8	5.1	6.4		
9	2.2	3.9		

occurring at the transition state, and bond length (dipole and dipolarophile) change occurs mainly after the transition state. Table 7 also gives the distorted energies for the ethylene and acetylene dipolarophiles. On average, ethylene/acetylene distortion accounts for ∼20% of the total distortion energy (for reactions with dipoles **1**−**6**), with acetylene requiring slightly more energy than ethylene (0.4−2.1 kcal/mol) to achieve the transition state geometry.

The distortion energy is related to the stability of the 1,3-dipole. In terms of valence bond ideas, the principal resonance structure, $X{=}Y^+{-}Z^-$, is stabilized by electronegative Z atoms, and the stability order of the dipole is oxide > imine > ylide. In orbital terms, the HOMO−LUMO gaps are largest for oxides, principally due to the low-energy HOMO that is concentrated at X and Z, while the LUMO coefficients are relatively small at X and Z.[8,9] Consequently, it is difficult to distort the oxides. On the other hand, with ylides, there is a small HOMO−LUMO gap, and it is easier to distort because there is some stabilizing HOMO−LUMO interaction upon bending. Figure 9 shows the HOMO−LUMO gap of the diazonium dipoles and the change that occurs upon distortion to the transition state geometry. Using RHF/6-311++(2d,p) orbital energies, the nitrous oxide HOMO orbital energy changes the most (∼0.5 eV) from the ground state to the

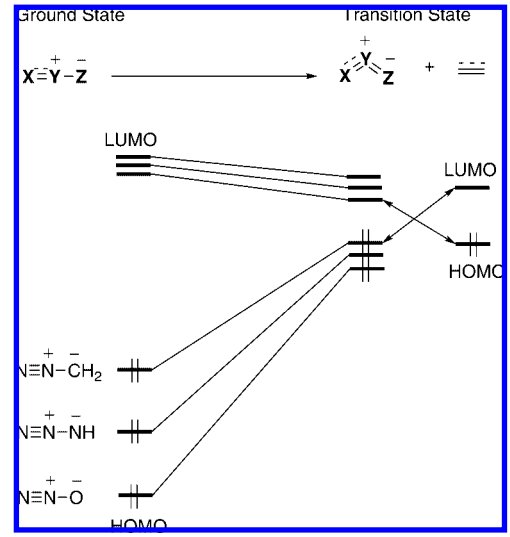

Figure 9. Diagram depicting the change in HOMO and LUMO energies of dipoles **1**−**3** upon distortion and FMO interactions at the transition state.

transition state, while the diazomethane ylide HOMO changes the least (∼0.2 eV). The narrow ground-state HOMO−LUMO gap of the ylide requires less energy to achieve the geometry where the HOMO−LUMO gap is sufficiently narrowed so that FMO interactions overtake the destabilizing distortion energy. Nitrous oxide requires a much larger change in energy to narrow its HOMO−LUMO gap to a similar extent.

The nature of the $X{=}Y^+$ fragment of the dipole also influences the activation barriers. When there is a nitrogen at the terminus, $N{=}N^+$ in diazonium dipoles, the dipole is stabilized compared to those with terminal carbons, $HC{=}N^+$ and $H_2C{=}NH^+$. This difference causes the diazonium dipoles to have significantly larger HOMO−LUMO gaps and larger barriers, while nitrilium and azomethine dipoles have similar barrier height. Again, this is due to the difference in distortion energy, and it is unrelated to overall reaction thermodynamics.

The only exception found for the monotonic decrease in activation enthalpies along each oxide, imine, ylide series was for nitrilium ylide, which has a barrier about 6 kcal/mol too high (Figure 2). Caramella and Houk previously discovered that the narrow HOMO−LUMO gap in the linear nitrilium ylide allows mixing of the π-HOMO orbital and σ^* C−H orbital, resulting in HOMO stabilization through a second-order Jahn−Teller effect that gives a bent ground-state geometry (Figure 4).[51] The ylide has HCN and CNC angles of 117° and 172°, respectively, as well as a slightly pyramidalized CH_2 group. B3LYP calculations predict that the linear-planar geometry is 12.6 kcal/mol higher in energy than the equilibrium bent geometry. The stabilized nonplanar ylide is thus more difficult to distort to the cycloaddition transition state geometry, resulting in a larger than expected barrier height.

In the appropriate distorted geometries the energy of the transition state depends upon $\Delta E_d^‡$ and $\Delta E_i^‡$. For the 18 parent reactions studied, $\Delta E_d^‡$ controls the reactivity patterns and the interaction energies are linearly related to these but only about 25% of the size of the distortion energy. Qualitatively, regardless of the exact form of the change in distortion energy ($\delta\Delta E_d$) with dipole angle (θ) deformation,

(51) Caramella, P.; Houk, K. N. *J. Am. Chem. Soc.* **1976**, *98*, 6397.

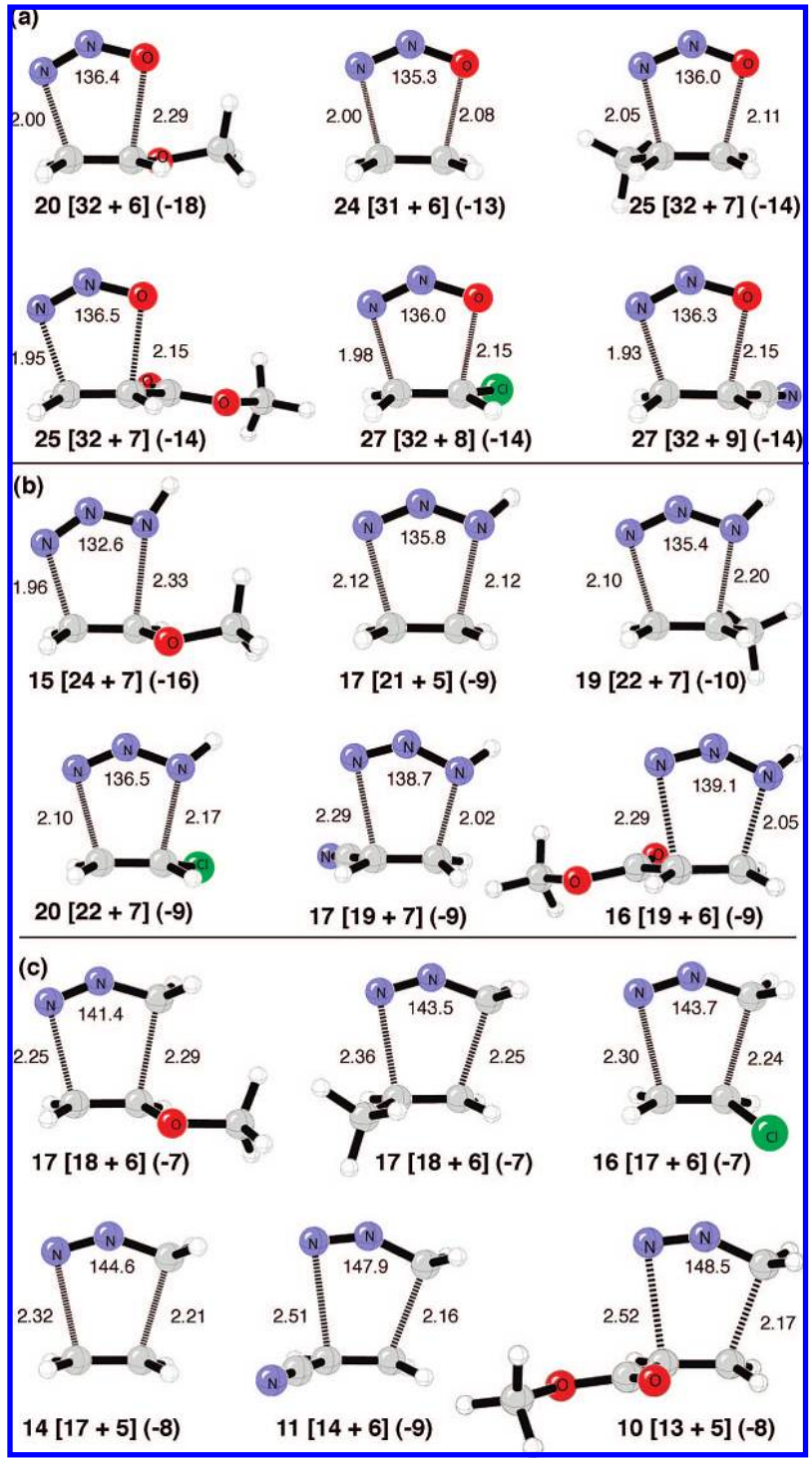

Figure 10. B3LYP/6-31G(d) $\Delta E^{\ddagger}$, [$\Delta E_d^{\ddagger}$ (dipole) + $\Delta E_d^{\ddagger}$ (alkene)], and ($\Delta E_i^{\ddagger}$) for the concerted transition structures of nitrous oxide, hydrazoic acid, and diazomethane with substituted ethylenes (kcal/mol).

the slope of the distortion energy change near the transition state, $\delta\Delta E_d^{\ddagger}/\delta\theta$, will be larger for oxides than ylides. Consequently, the interaction energy change at the transition state, $\delta\Delta E_i^{\ddagger}/\delta\theta$, must be larger for oxides than ylides and the $\Delta E_i^{\ddagger}$ at the transition state must also be larger for oxides than ylides.

Distortion/Interaction Energy Analysis of Substituted Dipolarophiles. The intermolecular interaction energy at the transition states for 1,3-dipolar cycloadditions consists of attractive orbital and electrostatic interactions plus repulsive closed-shell interactions. When transition state distortion energies are approximately the same for a series of different dipolarophiles, interaction energies (primarily FMO interactions) vary and become the controlling factor. To explore this more quantitatively, the distortion and interaction energies for a series of substituted alkenes (OMe, Me, Cl, CO_2Me, and CN) with dipoles **1**−**3** were computed. Figure 10 shows the lower energy regioisomeric[52] transition states and gives the activation, dipole distortion, alkene distortion, and interaction energies for each reaction.

For the electrophilic nitrous oxide dipole (Figure 10a), the electron-donating group OMe lowers the barrier by 4 kcal/mol compared to ethylene, while electron-withdrawing groups (Cl, CO_2Me, CN) increase the barrier by 1−3 kcal/mol. Although the alkene substituents polarize the π-orbitals and cause slightly more asynchronous transition state structures with methyl vinyl ether (MVE) and acrylonitrile (the two extremes), the dipole transition state angles change very little across the series of alkenes, resulting in dipole distortion energies that are nearly constant (within 1 kcal/mol). The largest interaction energy (18 kcal/mol) is for N_2O with MVE, resulting from the interaction of the low-lying LUMO in N_2O with the high-energy HOMO of MVE.[8,9] In the transition state with the electron-deficient alkene, acrylonitrile, the interaction energy is 4 kcal/mol less due to less charge-transfer from the alkene to N_2O. Although the differences in interaction energies, mainly the result of FMO differences, gives a qualitatively correct view of reactivity for this series of alkenes, the interaction energy differences account for approximately half of the change in barrier height. The MVE distortion energy is 6 kcal/mol, while the acrylonitrile distortion energy is 9 kcal/mol. The lower distortion energy for MVE is the result of polarization of the π-HOMO orbital onto the unsubstituted alkene carbon in the ground state; less distortion is required to create the necessary HOMO density at the nucleophilic carbon atom center to facilitate bonding to the electrophilic nitrogen atom of nitrous oxide in the transition state. For acrylonitrile, polarization of the alkene HOMO orbital onto the unsubstituted carbon is much less favorable and requires 3 kcal/mol more distortion energy. For this series of reactions, alkene distortion energies reinforce the reactivity pattern based on FMO interactions.

For the reactions of substituted alkenes with the ambiphilic hydrazoic acid (Figure 10b) the expected parabolic trend in barriers is observed;[6,8,9] electron-rich and electron-deficient alkenes lower the barrier ~2 kcal/mol compared to ethylene. The parent transition state with ethylene has a synchronous transition state with bond lengths of 2.12 Å. For MVE, the unsubstituted carbon atom of the alkene is clearly the nucleophilic center with a forming C−N bond length of 1.96 Å, while the substituted alkene carbon has a much longer transition state partial bond length of 2.33 Å with the NH terminal of azide. The electron-deficient alkenes, acrylonitrile and methyl acrylate, skew the partial bond lengths in the opposite direction compared to MVE. The NH terminal of azide is nucleophilic and unites with the unsubstituted alkene carbon center, giving partial bond lengths of 2.02 and 2.05 Å, respectively, while the other C−N partial bonds are both elongated to 2.29 Å. The substituents alter the dipole transition state angle to a small extent, from 133° to 139°. When azide acts as an electrophile with MVE, it must bend more and the dipole distortion energy increases by 3 kcal/mol compared to ethylene, while when azide acts as a nucleophile toward acrylonitrile and methyl acrylate, it bends less and the dipole distortion energy decreases by 2−3 kcal/mol. The alkene distortion energies are nearly the same for all substituted alkenes, although the parent reaction with ethylene requires 2 kcal/mol less alkene distortion energy. The interaction energies are widely different when comparing the transition states of electron-rich and electron-poor alkenes. For MVE, the 16 kcal/mol interaction energy is primarily the result of the $\text{alkene}_{\text{HOMO}}-\text{azide}_{\text{LUMO}}$ interaction. $\Delta E_i^{\ddagger}$ drops to only 9 kcal/mol for acrylonitrile and methyl acrylate, which mainly arises from $\text{alkene}_{\text{LUMO}}-\text{azide}_{\text{HOMO}}$ interactions. The $\Delta E_i^{\ddagger}$ for the reaction with ethylene is also 9 kcal/mol, and the total transition state distortion energy for the reactions with ethylene, acrylonitrile, and methyl acrylate are the same; these reactions are predicted to have barriers of 17, 17, and 16 kcal/mol, respectively.

Figure 10c shows the B3LYP transition structures for the reactions of the nucleophilic 1,3-dipole, diazomethane. As with hydrazoic acid, the transition structures are significantly influenced by the alkene substituent. Electron-donating groups tend to give more synchronous transition structures. In the transition state of N_2CH_2 with MVE, the C−C partial bond length is 2.29 Å and the C−N partial bond length is 2.25 Å. Electron-withdrawing substituents increase the influence of the nucleophilic methylene terminal of diazomethane, and the C−C bond is much more advanced than the C−N bond in the transition state. For example, the C−C partial bond in the transition state with methyl acrylate is 2.17 Å, while the C−N partial bond length is 2.52 Å. The dipole transition state angle also changes as a function of alkene substitution. In the transition state for MVE, the dipole is bent 4° more bent than in the transition state with ethylene (145°), while in the transition state with methyl acrylate, the dipole angle is bent 4° less (149°). The decrease in dipole angle decreases the dipole $\Delta E_d^{\ddagger}$ from 18 kcal/mol for MVE to 13 kcal/mol for methyl acrylate, and corresponds to the decrease in $\Delta E^{\ddagger}$ along the series from MVE (17 kcal/mol) to methyl acrylate (10 kcal/mol). The alkene distortion energy is almost unaffected by substitution, ranging from 5 to 6 kcal/mol, while the $\Delta E_i^{\ddagger}$ energies also have a narrow range (7−8 kcal/mol). In fact, the $\Delta E_i^{\ddagger}$ value for the reaction of electron-rich diazomethane with electron-poor methyl acrylate is only 1 kcal/mol larger than the reaction of diazomethane with the electron-rich MVE.

The reactions investigated in Figure 10 show that substituents can alter distortion and interaction energies, and there are three limiting situations: (1) $\Delta E_d^{\ddagger}$ is nearly constant, and reactivity is dictated by $\Delta E_i^{\ddagger}$, exemplified in the case of reactions with nitrous oxide. (2) $\Delta E_i^{\ddagger}$ is similar across the series of alkenes, and dipole, alkene, or both distortion energies control reactivity. (3) Substituents influence both $\Delta E_d^{\ddagger}$ and $\Delta E_i^{\ddagger}$. As in the reactions with hydrazoic acid, distortion energy changes typically reinforce the reactivity patterns based on FMO interactions.

Conclusion

Surprising quantitative trends in the activation barriers for 1,3-dipolar cycloadditions have led to new interpretations of reactivity. Previously unrecognized are the (1) monotonic decrease of activation energy along the series oxide, imine, and ylide for the diazonium, nitrilium, and azomethine betaine classes of 1,3-dipoles; (2) nitrilium and azomethine betaines with the same trio of atoms have identical barriers; (3) barrier heights for the cycloadditions of a given 1,3-dipole with ethylene and acetylene are nearly the same despite very different reaction

(52) Here we are concerned with dipolarophile reactivity, not regioselectivity differences. Rastelli and co-workers have previously shown that dipolarophile distortion energy is important for diasterofacial selectivity in 1,3-dipolar cycloadditions with cyclobutenes. See for example: (a) Bagatti, M.; Rastelli, A.; Burdisso, M.; Gandolfi, R. *J. Phys. Org. Chem.* **1992**, *5*, 819. (b) Bagatti, M.; Ori, A.; Rastelli, A.; Burdisso, M.; Gandolfi, R. *J. Chem. Soc. Perkin Trans. 2* **1992**, 1657. (c) Rastelli, A.; Bagatti, M.; Ori, A.; Gandolfi, R.; Burdisso, M. *J. Chem. Soc. Faraday Trans.* **1993**, *89*, 29. (d) Rastelli, A.; Bagatti, M.; Gandolfi, R. *J. Chem. Soc. Faraday Trans.* **1993**, *89*, 3913.

thermodynamics and FMO energy gaps. The energy to distort the 1,3-dipole and dipolarophile to the transition state geometry is the major factor controlling the reactivity differences of 1,3-dipoles. Interaction energies between the 1,3-dipole and the dipolarophile differentiate reactivity for a series of substituted alkenes when the distortion energies are nearly constant. This distortion/interaction model provides a new way of understanding of reactivity trends for dipolar cycloadditions and should be applicable to bimolecular reactions in general.

Acknowledgement. We are grateful to the National Science Foundation for financial and supercomputer support. D.H.E. acknowledges a traineeship (NSF IGERT: Materials Creation Training Program (DGE-0114443). The computations were performed using National Center for Supercomputing Applications (NCSA) resources and the UCLA Academic Technology Services (ATS) Hoffman Beowulf cluster. We are also grateful to Rolf Huisgen, Rudolph Marcus, Raymond Firestone, and Reiner Sustmann for helpful comments.

Supporting Information Available: Absolute energies and Cartesian coordinates of stationary points. Complete ref 27. This material is available free of charge via the Internet at http://pubs.acs.org.

JA800009Z